From Molecular Dynamics to Supramolecular Organization: The Role of PIM Lipids in the Originality of the *Mycobacterial* Plasma Membrane

Chelsea M. Brown[1], Robin A. Corey[2], Ya Gao[3], Yeol Kyo Choi[4], Martine Gilleron[5], Nicolas Destainville[6], Elizabeth Fullam[1], Wonpil Im[3,], Phillip J. Stansfeld[1,7,*,+], Matthieu Chavent[5,*,+]*

[1] School of Life Sciences,
University of Warwick,
Coventry,
CV4 7AL,
UK

[2] Department of Biochemistry,
University of Oxford,
Oxford,
UK

[3] School of Mathematics, Physics and Statistics,
Shanghai University of Engineering Science,
Shanghai 201620,
China

[4] Department of Biological Sciences,
Department of Chemistry,
Department of Bioengineering,
Lehigh University,
Pennsylvania 18015,
USA

[5] Institut de Pharmacologie et Biologie Structurale,
CNRS, Université de Toulouse,
205 route de Narbonne,
31400, Toulouse,
France

[6] Laboratoire de Physique Théorique,
CNRS, Université Paul Sabatier,
31062 Toulouse,
France

[7] Department of Chemistry,
University of Warwick,
Coventry,
CV4 7AL,
UK

+ equal contribution

*to whom correspondence should be addressed:
e-mail: wonpil@lehigh.edu
phone: +1 (0) 610-758-4524

e-mail: phillip.stansfeld@warwick.ac.uk
phone: +44 (0) 2476523864

e-mail: matthieu.chavent@ipbs.fr
phone: +33 (0) 5-61-17-59-00

Abstract

Mycobacterium tuberculosis (*Mtb*) is the causative agent of tuberculosis, a disease that claims ~1.5 million lives annually. The current treatment regime is long and expensive, and missed doses contribute to drug resistance. There is much to be understood about the *Mtb* cell envelope, a complicated barrier that antibiotics need to negotiate to enter the cell. Within this envelope, the plasma membrane is the ultimate obstacle and is proposed to be comprised of over 50% mannosylated phosphatidylinositol lipids (phosphatidyl-*myo*inositol mannosides, PIMs), whose role in the membrane structure remains elusive. Here we used multiscale molecular dynamics (MD) simulations to understand the structure-function relationship of the PIM lipid family and decipher how they self-organize to drive biophysical properties of the *Mycobacterial* plasma membrane. To validate the model, we tested known anti-tubercular drugs and replicated previous experimental results. Our results shed new light into the organization of the *Mycobacterial* plasma membrane and provides a working model of this complex membrane to use for *in silico* studies. This opens the door for new methods to probe potential antibiotic targets and further understand membrane protein function.

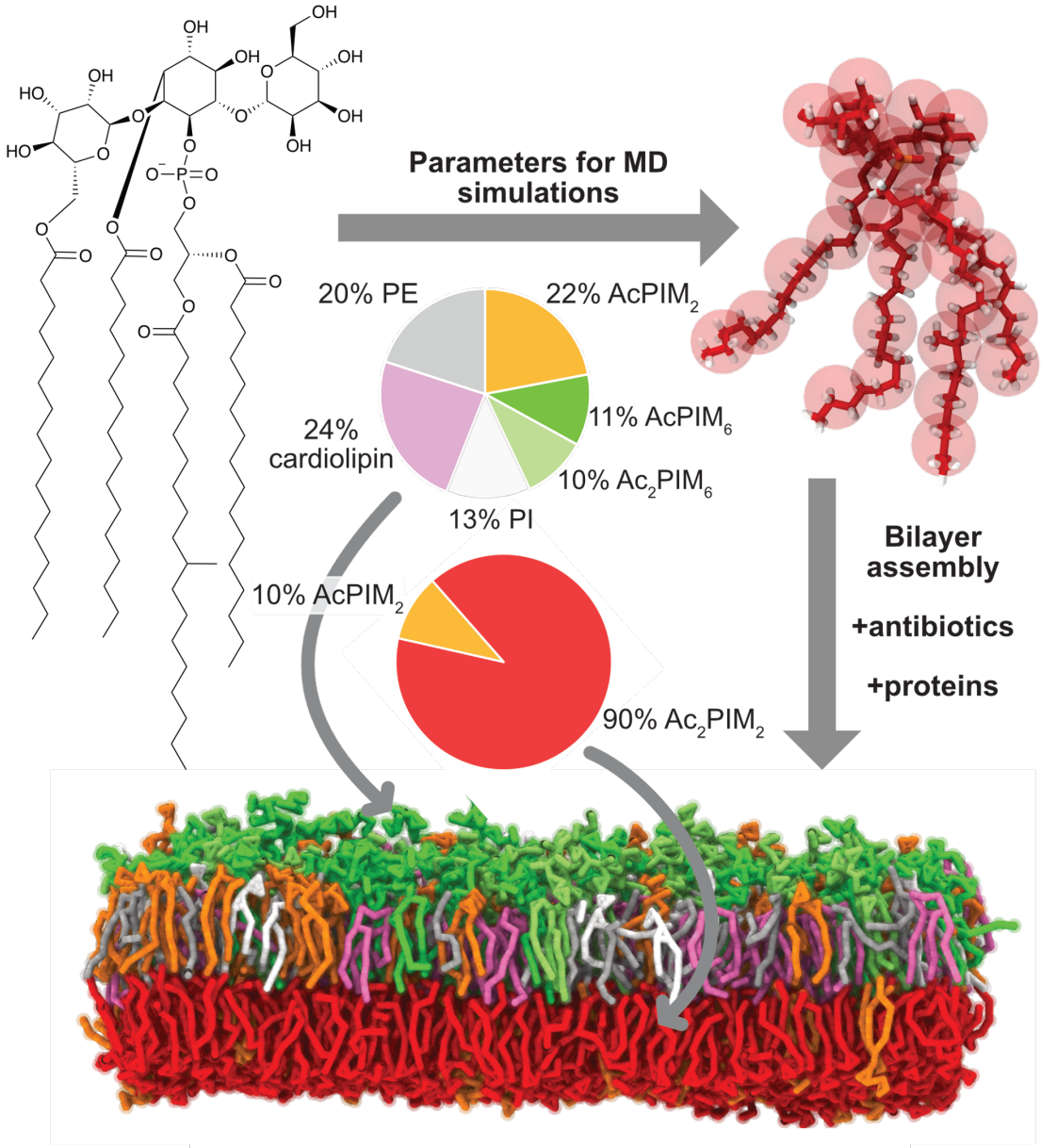

Asymmetric *Mycobacterial* plasma membrane

Introduction

Tuberculosis (TB) is caused by *Mycobacterium tuberculosis* (*Mtb*). In 2020 alone, there were an estimated 10 million new *Mtb* infections, leading to 1.5 million deaths[1]. Thus, *Mtb* is one of the world's leading infectious killers, despite the availability of both a treatment regime and a vaccine. The current course of antibiotics for drug susceptible TB cases can last as long as 6 months and consists of four drugs given in combination[2]. This is not only expensive and demanding for the patient, but also encourages non-compliance that contributes towards the rise in multi-drug resistant TB[1]. It is obvious that new treatments and a better vaccine are needed to meet the World Health Organization's 'End TB Strategy'. Their plan aims to reduce TB-related deaths by 90% by 2030, and thereby curtail the enormous public health cost caused by TB[3]. The COVID-19 pandemic has undone some of the progress that had been made in the treatment of TB as fewer people were able to be diagnosed or access medication[4], which may create a worldwide surge of untreatable cases. Thus, there is a pressing need for innovative research into the mechanisms of *Mtb* virulence and its ability to survive within the host for extended periods to help develop alternative intervention strategies.

One issue in developing new treatments for TB is the complexity of the *Mycobacterial* cell envelope[5, 6]. This cell envelope consists of an array of lipids contributing to both hydrophobic and polar regions of various thicknesses and densities, making it extremely challenging to predict how molecules will cross this barrier and enter the cell. The cell envelope is generally described as having four distinct layers: the *mycomembrane* (or outer membrane) comprised of mycolic acids and phthiocerols, an arabinogalactan-peptidoglycan layer, the periplasmic space containing lipomannan (LM) and lipoarabinomannan (LAM) and finally the inner membrane, or the plasma membrane[7]. The *Mycobacterial* plasma membrane has a key role in controlling nutrient/antibiotic uptake and contains important membrane proteins that are targets for antitubercular drugs[8], such as SQ109 that inhibits the transporter MmpL3[9]. On the other hand, we are becoming increasingly aware of how *Mtb* plasma membrane organization, such as the formation of functional membrane microdomains[10], can affect the survival ability of *mycobacteria*. Therefore, understanding the molecular organization and dynamics of the *Mtb* plasma membrane is essential for developing effective drug candidates.

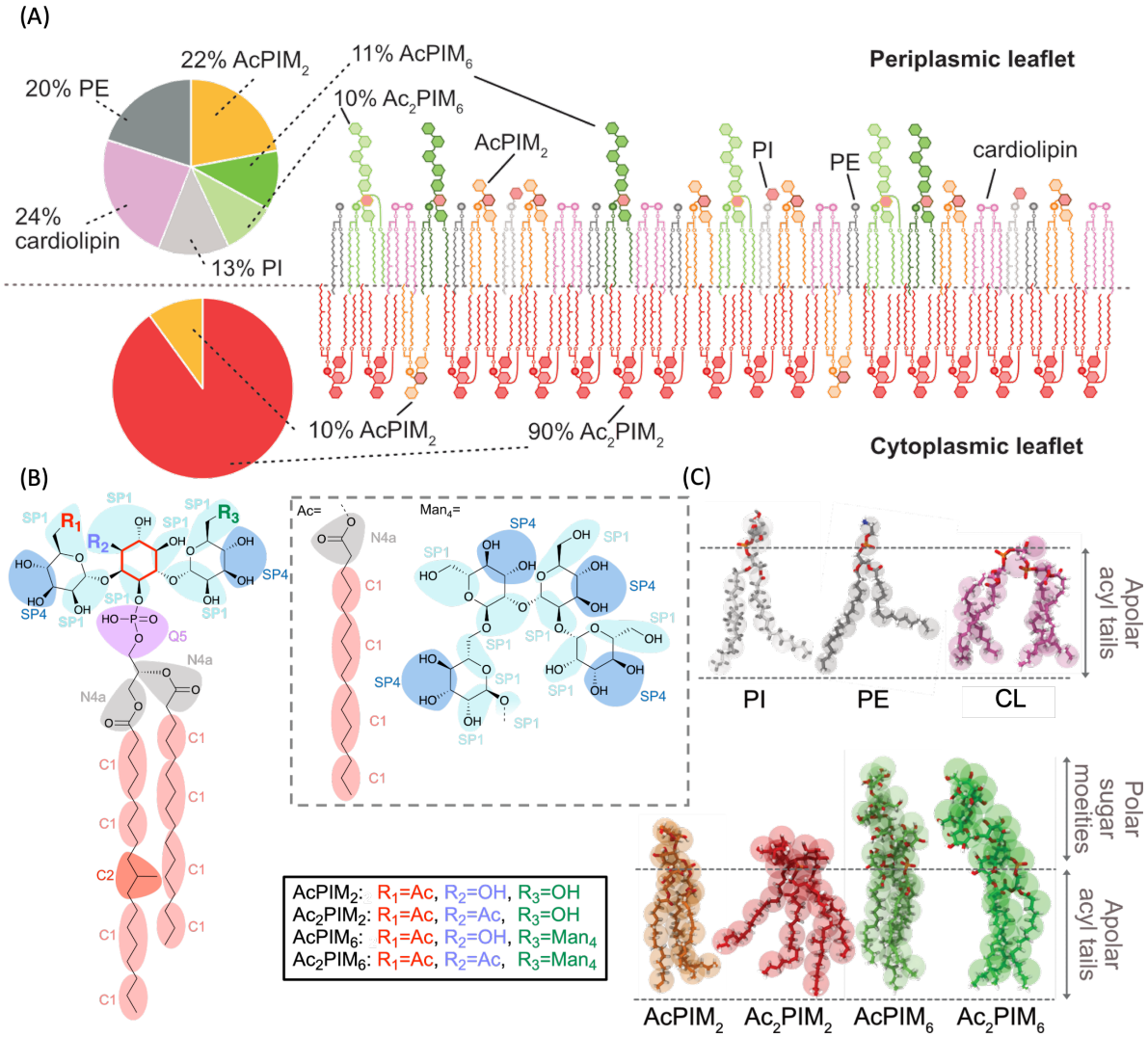

Figure 1: The structure of the *Mycobacterial* plasma membrane and PIM lipids. (**A**) Schematic of the plasma membrane of *Mycobacteria* with the compositions previously defined[11]. (**B**) Schematic of the core of the PIM lipids found in *Mycobacteria* with the groupings for CG overlaid. The inositol core is highlighted in red. The bead types for MARTINI 3 are shown beside. (**C**) Overlay of the AT (sticks) and CG (spheres) models for each lipid, with chemical characteristics shown to the right.

The *Mycobacterial* plasma membrane is composed of a variety of lipids and glycolipids (**Figure 1A**): cardiolipin (CL), phosphatidylethanolamine (PE), phosphatidyl-*myo*inositol (PI), trehalose monomycolate (TMM) and phosphatidyl-*myo*inositol mannosides (PIMs)[11], with the PIMs accounting for over half the dry weight of the plasma membrane lipids[11]. These lipids comprise of a modified phosphatidylinositol core decorated with two mannose residues and one acyl chain (**Figure 1B**). Furthermore, additional modifications of an acyl group and up to 4 mannose sugars can be added to the core headgroup[12, 13] (**Figure 1B** and **SI Figure 1**). The plasma membrane is proposed to be asymmetric[11], with Ac_2PIM_2 being the

dominant species in the cytoplasmic leaflet accompanied by $AcPIM_2$, while the periplasmic leaflet is more varied, containing $AcPIM_2$, $AcPIM_6$, Ac_2PIM_6, CL, PI, PE and TMM[5, 11, 14, 15]. PIM_6 lipids can be further modified to LM and LAM that make up the bulk of the periplasmic space[16]. Due to the complexity of the *Mycobacterial* cell envelope, the dynamics and properties of the plasma membrane alone is extremely difficult to probe experimentally.

Lipid interactions with proteins can be key for understanding mechanisms of action and potential new targets for drugs[17]. Modulation of human serotonin receptors by cholesterol[18] and gating of bacterial Kir potassium channels by anionic lipids are observed experimentally[19], but limited effects of lipids on *Mycobacterial* proteins are determined. Structures of important *Mycobacterial* membrane proteins are starting to emerge[20, 21], but experimental information about the surrounding lipids and their interactions are difficult to resolve.

Molecular dynamics (MD) simulations have been used to study lipid organization and the formation of domains on a large scale[22] as well as comparative studies of eukaryotic, prokaryotic, and archaeal membranes[23]. Despite this, at the time of writing, there are no complete models of the *Mycobacterial* plasma membrane that capture the asymmetry and the range of complex lipids[24]. As a result, *Mycobacterial* membrane proteins cannot be simulated in a native environment. There are growing tools to embed proteins in membranes *in silico*[25, 26 27, 28], meaning that their behavior can be studied using MD simulations. Such simulations have shown that phosphatidylinositol phosphate lipids (PIPs) can modulate ephrin receptors in humans[29], while CL can bind to a range of *E. coli* membrane proteins[30]. It is therefore timely to develop models of the major phospholipids of the *Mycobacterial* envelope for application in MD simulations. This will enable studies into the dynamics of the membrane, specific lipid interactions with integral membrane proteins and diffusion of antibiotics across this barrier. By performing simulations of these systems with a coarse grained (CG) representation, key interactions may be probed over a large timescale and established prior to conversion to atomistic (AT) resolution for further in-depth evaluation.

Herein, multiscale simulations were used to analyze the structure-function relationship of the four main PIM lipids ($AcPIM_2$, Ac_2PIM_2, $AcPIM_6$ and Ac_2PIM_6) found in the *Mycobacterial* membrane. An asymmetric bilayer containing these lipids was assembled and simulated, showing the stability of this composition. A global analysis

of the membrane shows lipid diffusion and no excessive clustering throughout the simulations. We provide CG structures of antibiotics known to interact with the membrane and membrane proteins and replicate experimental results[31]. Overall, we have developed a robust representation of the *Mycobacterial* plasma membrane.

Methods

Building the coarse-grained lipid parameters

The CG models of the lipids were parametrized for the newly released MARTINI 3 force field[32] and generated using the protocol described for small molecules[33] on the MARTINI website (http://cgmartini.nl/index.php/martini-3-tutorials/parameterizing-a-new-small-molecule). The bead types and mapping to the PIM molecules were performed manually, comparing with the recently published CG model of PI[34]. Atoms were grouped according to functional groups, in sets of 3-5 non-hydrogen atoms. The CG mapping of Ac_xPIM_x is shown in **Figures 1B,C**. The parameter files that describe the bonds, constraints, and angles were assembled based on the previously described data[32, 34, 35] as an initial estimate.

Simulations of each lipid were set up using a modified version of *insane.py* python script[27], embedding one copy of a PIM lipid in a 10 x 10 nm^2 phosphatidylcholine (PC) bilayer. The system was solvated with water and neutralized with 150 mM NaCl, followed by minimization using the steepest descents algorithm. The system was then simulated for 3 μs using a timestep of 20 fs at 310 K. The lipids, solvent and ions were temperature coupled separately. The velocity rescale[36] and Parrinello-Rahman[37] coupling methods were used with the time constants τ_T = 1.0 ps and τ_p = 12.0 ps for temperature and pressure, respectively. Simulations were run using GROMACS version 2021.3[38]. The reaction-field algorithm[39] was used for electrostatic interactions with a cut-off of 1.1 nm. A single cut-off of 1.1 nm was used for the van der Waals interaction. Five repeats were performed for each lipid (**SI Figure 2**).

Generating atomistic data

Parameters for the AT Ac_xPIM_x lipids were generated using the CHARMM force field[40]. The CHARMM-GUI[41] server was used to set up the lipid systems for GROMACS with the CHARMM36m force field[42, 43]. One PIM lipid was embedded in an 8 x 8 nm^2 PC

bilayer. The system was solvated with 150 mM NaCl and minimized and equilibrated as per the Membrane Builder workflow[28]. The system was further minimized using the steepest descents. Simulations were run for 2 μs using a timestep of 2 fs at 310 K. The lipids, solvent and ions were temperature coupled separately. The velocity rescale[36] and C-rescale coupling methods were used with the time constants τ_T = 0.1 ps and τ_p = 1.0 ps for temperature and pressure, respectively. Simulations were run using GROMACS version 2021.3[38]. The particle mesh Eward (PME)[44] method was used for electrostatic interactions with a cut-off of 1.2 nm. A single cut-off of 1.2 nm was used for the van der Waals interaction. Three repeats were performed for each lipid (**SI Figure 2**).

Refining coarse-grained parameters

The AT and CG representations of the four main PIM lipids are shown in **Figure 1C**. The distributions of the distances and angles were measured using the *gmx* tools (*distance*, *gangle* and *analyze*). For the AT simulations, the atoms were grouped according to their mapping and its center of geometry was used for calculations. The values for each bond/constraint and angle were iteratively refined based on the comparison of probability distribution, and the results are summarized in **SI Figures 3-8**. When there was agreement between the AT and CG data, the solvent accessible surface area was measured using the *gmx sasa* tool to verify that the models behaved the same (**SI Figure 8C**). Diffusion, shape of the lipids, clustering of ions and aggregation were also measured on a single lipid level (**SI Methods** and **SI Figures 9-17**). It is important to note that there are no energy barriers for the dihedral angles.

Measuring area per lipid

Before setting up the complete bilayer system, the area per lipid was measured. The simulations were assembled as described above for CG, using a homogenous Ac_xPIM_x membrane (**SI Figure 2**). The area of *XY*-dimension was measured using *gmx energy* and then dividing the area by the number of lipids in one leaflet over the course of the trajectory, and final values extracted using *gmx analyze*, as per the protocol described on the MARTINI website (http://cgmartini.nl/index.php/tutorials-general-introduction-gmx5/bilayers-gmx5#Area-per-lipid).

Bilayer composition and set-up

The ratio of lipids in each bilayer was obtained by using their molecular weight and the previously reported dry masses[11] of the individual lipids, and the exact calculations can be seen in **SI Figure 18**. Since the specific apolar lipids were not named, they were not included in this study. TMM was not included as there is no available refined atomistic model, the behavior of the mycolic acid is predicted to be complicated[45], and there is a relatively small proportion of TMM predicted to be present in the membrane. The exact composition of the simulated plasma membrane is shown in **Figure 1A**.

The PI and PE lipids in *Mycobacteria* are slightly different in structure to the corresponding *E. coli* lipids described in the MARTINI force field[34 32]: a methyl group replaces the alkene found in one of the acyl chains (**SI Figure 1**). Before assembling the membrane, the parameters for these lipids were modified by adapting the refined Ac_2PIM_2 acyl tail parameters and changing the existing tail. The CL parameters were transferred over from the MARTINI 3 beta force field[30].

Simulations of the bilayer were set up using a modified version of *insane.py* python script[27] using the composition shown in **Figure 1A**, where the area per lipid for the periplasmic membrane was set to 0.92 nm^2 and the cytoplasmic leaflet set to 1.13 nm^2. The systems were then treated the same as described for the initial CG systems with added equilibration steps as per the Membrane Builder workflow[28] before the production simulation. There were two types of system assembled. The first one has a simulation box size of 20 x 20 x 15 nm^3 and one repeat was performed for 10 μs at 290 K, 300 K, 310 K, 320 K and 350 K. The second one has a box size of 50 x 50 x 15 nm^3 and a single repeat was performed for 10 μs at 310 K (**Figure 2A** and **SI Figure 2**).

Behavior of the membrane

To calculate the bending rigidities, the strategy proposed by Fowler *et al*.[46] to extract the bending modulus from CG simulations was followed. The membrane midplane position in Monge representation was determined by extracting the coordinates of all CG beads at the extremities of lipid fatty acid chains. Using a built-in function of the Mathematica software package, the positions were interpolated to get a smooth function before Fourier-transforming with a fast Fourier transform algorithm. From the so-obtained Fourier modes, the spectral density (or power spectrum) was estimated:

$$S(q) = L^2 k_B T \left(1/(\kappa q^4) + 1/\left(\sigma_p r q^2\right)\right)$$

for a tensionless membrane, where L^2 is the projected area in the (x, y) plane, $k_B T$ is the thermal energy and $\sigma_p r \sim 0.1$ J/m^2 is the tension associated with lipid protrusions at the nanometer scale. $S(q)q^4$ was plotted as a function of q and fit it with a second order polynomial $P(q) = a + bq^2$, from which estimates of κ (and $\sigma_p r$ if needed) were obtained (**SI Figure 19**). The error bars are standard deviations provided by the fitting function in Mathematica.

Diffusion, bilayer thickness and number of neighbors was measured using LiPyphilic[47] (**Figures 2B,C**, **SI Methods** and **SI Figure 20**). The xy-positions of single lipids were tracked with PLUMED[48] (**Figure 2B**). Area per lipid for the membrane was calculated using FATSLiM[49] (**Figure 2D**). The density of each constituent was measured using *gmx density* (**Figure 2E**). Plots were created using Matplotlib[50].

Antibiotic simulations

Bedaquiline (BDQ) and isoniazid (ISZ) were mapped to CG using PyCGTOOL[51] following 200 ns AT simulations with parameters from CHARMM-GUI[52] (**Figure 3A**).

BDQ was first simulated with the *Mycobacterial* membrane alone to confirm association with the membrane (**SI Figures 2,21**). The *Mtb* a- and c-subunits of F-ATPase, BDQ's target in the *Mycobacterial* membrane, was modelled using SwissModel[53] based on a structure from *Mycobacterium smegmatis*[31] (PDB: 7JGC, **Figure 3C** and **SI Figures 22A,B**). The sequence identity at the amino acid level between *Mtb* and *M. smegmatis* for the F-ATPase was calculated using Clustal Omega[54] at 80% and 72% for c- and a-subunits, respectively. The system with the protein in a *Mycobacterial* membrane was assembled using martinize2[55], memembed[56] and the modified *insane.py* python script[27], with eight molecules of BDQ placed either in the periplasmic or cytoplasmic leaflet with five repeats in each membrane (**SI Figure 2**). Simulations were run for 10 μs using the same setting as described above. The xyz-positions of BDQ, the lipids and the backbone beads were tracked over the course of the simulations with PLUMED[48] and plotted with Matplotlib[50], and the results are shown in **Figure 3D** and **SI Figures 22C,D, 23**. The density of each constituent was measured using *gmx density* and plotted using Matplotlib[50] and the results are shown in **Figure 3E** (with representative positions shown in **Figure 3F**). The interaction of BDQ with the protein was calculated using

PyLipID[57] (**Figure 3G** and **SI Figures 24,25**). The same simulation set up was performed with a model *E. coli* (simple) membrane (75% PE, 15% PG, 10% CL) and the z-position of BDQ can be seen in **SI Figure 26**.

PMF calculations

The potential of mean force (PMF) calculations were run as previously described[58]. For the F-ATPase-BDQ PMF, a representative pose of BDQ bound to the protein was produced using PyLipID from equilibrium simulations and built into a 12 x 20 x 11 nm *Mycobacterial* membrane and minimized and equilibrated, as described above. Light (50 kJ/mol/nm^2) *xy* positional restraints were added to Ala 66 on three c-subunits to prevent the protein from rotating in the membrane. Following 50 ns of equilibration, the BDQ was steered away from the protein along the *y* axis at a rate of 1 nm/ns with a 1,000 kJ/mol/nm^2 umbrella potential. Frames were extracted at 0.1 nm spacing along this coordinate to seed a total of 58 x 1.5 μs production simulations with a static 1,000 kJ/mol/nm^2 umbrella potential imposed to keep the system in the same position along the reaction coordinate. The PMF profiles were then constructed using the weighted histogram analysis method (*gmx wham*) in GROMACS[59, 60], and employing 200 rounds of Bayesian bootstrapping to report statistical accuracy (**Figure 3H**).

For the membrane crossing PMFs, BDQ or ISZ was placed free in the solvent phase, 7 nm away from the membrane periphery in either an *Mycobacterial* or *E. coli* membrane. The drug was then steered towards and through the membrane and into the solvent phase on the other side. Windows were extracted, simulated (1 μs for ISZ per window and 2 μs per window for BDQ) and analyzed as described above (**Figure 3B**). The –cycl option was imposed when running *gmx wham.*

Results

Parameterization & lipid properties

After refinement of the CG parameters, the probability distributions of bonds and angles from the CG and AT simulations align well (**SI Figures 3-8**), showing that the behavior of the acyl chains is similar to other phospholipids[27]. The Ac_xPIM_x aggregation in the AT and CG simulations is comparable and shows no permanent clustering. When lipids did come into contact, all areas of the molecule appear to play an equal role in the interactions (**SI Figures 15,17**). The interactions are not dominated

by the sugars, as was seen with the previous iteration of the MARTINI 2 force field[61]. The PIM lipids show a higher affinity for ions than PC in CG simulations but the effect is less apparent in AT simulations (**SI Figure 14**). While the ion concentrations were the same, the number of ions in the simulation box were different (an order of magnitude higher for CG), which could explain these results. Overall, CG simulations of these lipids behave similarly to AT models (interactions with ions as a minor exception), therefore opening the door to significantly longer simulations by decreasing the degrees of freedom in the system.

The area per lipid in CG for each species in a PC bilayer was found to be 0.93 nm^2 ($AcPIM_2$), 1.15 nm^2 (Ac_2PIM_2), 1.01 nm^2 ($AcPIM_6$), 1.14 nm^2 (Ac_2PIM_6), 0.6 nm^2 (PI), 0.55 nm^2 (PE) and 1.25 nm^2 (CL). It is interesting that the average area per lipid for the cytoplasmic and periplasmic leaflets slightly differ (1.13 nm^2 and 0.93 nm^2, respectively), suggesting that the properties of these leaflets could vary. The diffusion coefficients for each PIM species in a PC bilayer at 310 K are as follows: 6.7 x 10^{-7} cm^2/s ($AcPIM_2$), 1.1 x 10^{-7} cm^2/s (Ac_2PIM_2), 7.6 x 10^{-7} cm^2/s ($AcPIM_6$), 6.5 x 10^{-7} cm^2/s (Ac_2PIM_6) (**SI Figure 9**). The difference between $AcPIM_x$ and Ac_2PIM_x shows the effect of the extra acyl tail in terms of how freely these lipids diffuse through the membrane.

The shape of the lipids is approximately the same from AT to CG (**SI Figures 10-13**), which agrees with the comparison of the surface areas (**SI Figure 8C**) and the sugar-phosphate z-distances in Ac_xPIM_6 (**SI Figures 5C,7C**). The additional mannose moieties project upwards away from the membrane in both set of simulations. Interestingly, the tail region of the lipid is measured to occupy approximately the same amount of space with three or four acyl chains. This is likely due to the placement of the fourth tail, projecting downwards from the inositol sugar (as highlighted in red in **Figure 1B**) and hence inhabiting space close to the other acyl chains.

Mycobacterial membrane biophysical properties

Traditionally, in MD simulations of bacterial membranes, symmetric bilayers are used to resemble the *E. coli* plasma membrane. On the contrary, the *Mycobacterial* plasma membrane is an asymmetric bilayer. The published composition of the *Mycobacterial* plasma membrane[11] (**Figure 1**) (excluding apolar lipids and TMM) was used to assemble the bilayer. This bilayer was found to be stable during the course of 10 μs simulation, providing some evidence to confirm what has previously been reported in the literature[7, 11]. This can be seen in **SI Movie 1**. The thickness of the plasma

membrane has been imaged to be between 6.3 nm (*Mycobacterium bovis*) and 7 nm (*Mycobacterium smegmatis*)[62-64], which is slightly larger than the sugar thickness seen in our simulations at 5.3 ± 0.1 nm (**Figure 2E**), although in the density plot thicknesses of up to 7 nm were observed at the extremes. The difference could be due to the lack of LAM and LM present in this membrane model and will be interesting for further investigation.

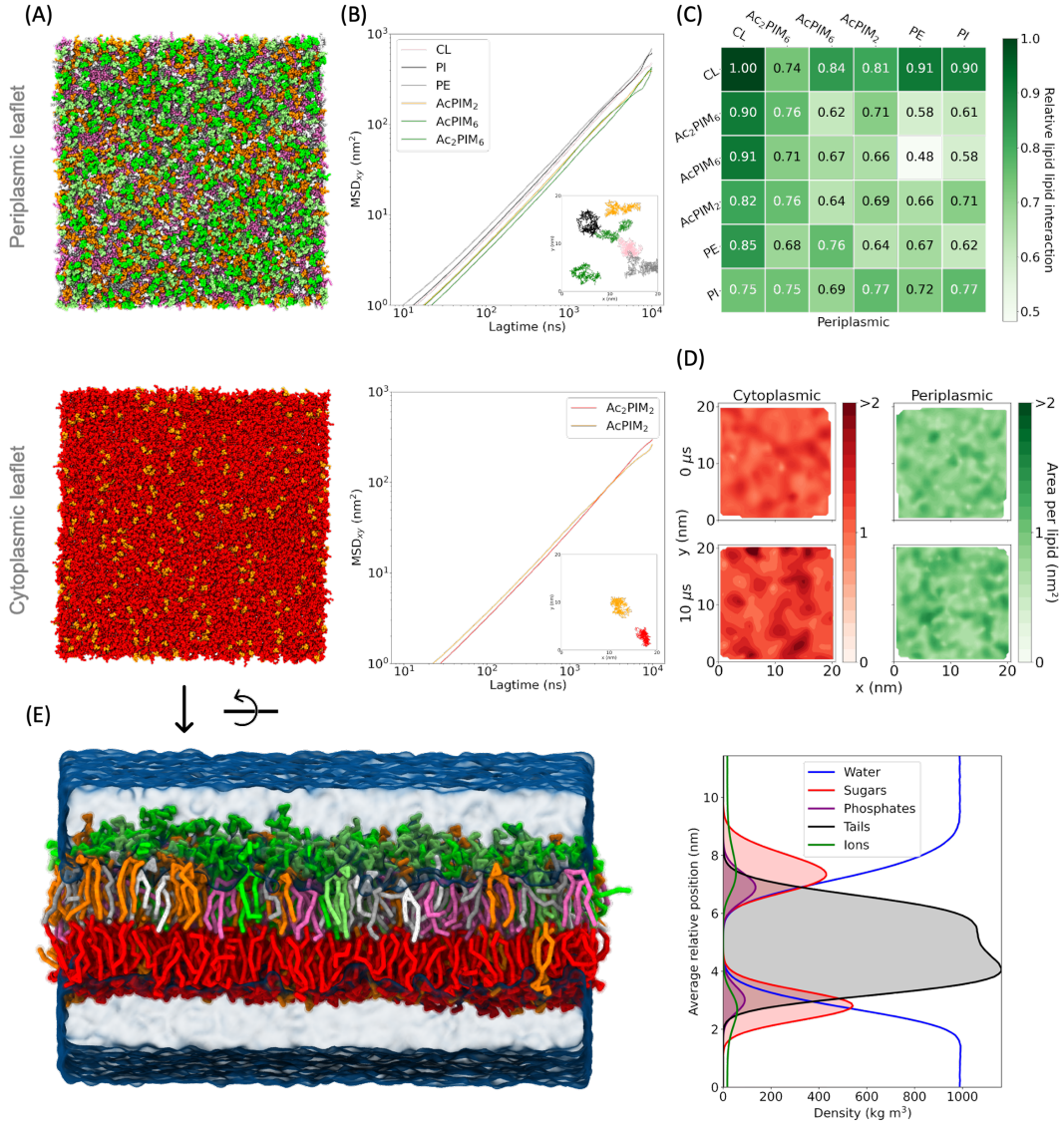

Figure 2: A *Mycobacterial* membrane model. (**A**) Snapshots of the periplasmic and cytoplasmic leaflets whose compositions are: $AcPIM_2$ 22%, $AcPIM_6$ 11%, Ac_2PIM_6 10%, CL 24%, PE 20% and PI 13% (periplasmic leaflet) and $AcPIM_2$ 10% and Ac_2PIM_2 90% (cytoplasmic leaflet). The system size is 50 x 50 x 15 nm. (**B**) Mean squared displacement (MSD_{xy}) (nm^2) as a function of lagtime (ns) for each lipid type in the periplasmic and cytoplasmic leaflets. The inserts show the position of the phosphate group of each lipid type over the last 500 ns of the simulation. (**C**) Relative number of neighbors of each lipid type for the periplasmic membrane. (**D**) Contour plots of the area per lipid (nm^2) in each leaflet at the

starting frame (upper) and final frame (lower) of the simulation. A darker color indicates a larger area per lipid. (**E**) Side view of the membrane with each lipid type depicted in a different color as shown in **Figure 1A**. The density plot shows the density of water, sugar groups, phosphate groups, tail groups and ions over the simulation box.

To test the phase behavior of this membrane, we performed simulations at various temperatures ranging from 290 K to 350 K. For the whole range of temperatures, lipids are in the liquid phase and diffuse freely (**SI Figure 20**). The diffusion coefficients for each species in the periplasmic leaflet at 310 K are as follows: 9.9 x 10^{-8} cm^2/s ($AcPIM_2$), 6.9 x 10^{-8} cm^2/s ($AcPIM_6$), 1 x 10^{-7} cm^2/s (Ac_2PIM_6), 1.3 x 10^{-7} cm^2/s (PI), 1.5 x 10^{-7} cm^2/s (PE) and 1.2 x 10^{-7} cm^2/s (CL). In the cytoplasmic leaflet, the values are 6.1 x 10^{-8} cm^2/s ($AcPIM_2$) and 8.1 x 10^{-8} cm^2/s (Ac_2PIM_2). Compared to isolated PIMs in a PC membrane, the diffusion in this plasma membrane is roughly one order of magnitude slower for the PIMs. $AcPIM_2$, which is the only lipid in both leaflets, has approximately the same diffusion coefficient in both leaflets. Using a previously reported mammalian plasma membrane[22], the diffusion coefficients of PE and PI were calculated to be 3.3 x 10^{-7} cm^2/s and 2.8 x 10^{-7} cm^2/s, showing that the diffusion in the mammalian membrane is equivalent to that in the *Mycobacterial* plasma membrane. Comparing *a Mycobacterial* membrane to a pure PC membrane and this mammalian plasma membrane, the membrane stiffness is significantly lower at κ =8.2 k_BT compared to 13.9 k_BT and 19.1 k_BT for the mammalian and PC membranes, respectively (**SI Figure 19**), highlighting a specific dynamical behavior for the *Mycobacterial* plasma membrane.

Lipid clustering was moderate and membrane composition remained heterogenous over the course of each 10 μs simulation (**Figure 2B**). This can also be seen in **Figure 2C** where the number of surrounding lipids of the same type for each species in the periplasmic membrane is roughly equivalent to that of any other lipid species. The distribution of the area per lipid in the membrane also suggests high heterogeneity (**Figure 2D**). The average area per lipid in the membrane over the course of the simulation is 0.89 nm^2 and 1.18 nm^2 for the periplasmic and cytoplasmic leaflets, respectively. Thus, the cytoplasmic leaflet appears to be a little denser than the periplasmic leaflet. This can be related to the packing of the four acyl chains of Ac_2PIM_2 lipids present in high concentration in this leaflet[65]. A movie for the change in

area per lipid for each leaflet over the course of the simulation can be found in **SI Movies 2,3**.

As was seen for the individual lipids in CG the overall bilayer attracted ions, both Cl^- and Na^+ concentration was much higher close to the bilayer, especially around the sugar head groups compared to bulk solution (**Figure 2E**). It has been shown that lipid-ion interactions can affect the biophysical properties of the membrane, such as fluidity and stiffness, as well as the structure, which could modify the interaction with proteins present[66].

Asymmetric interaction of the membrane with antibiotics

We were then interested to test how the organization of this membrane may affect the behavior of other molecules. We first tested two antibiotics: Isoniazid (ISZ) and Bedaquiline (BDQ) (see the modelling of these molecules in the Methods section). ISZ is a first line anti-tubercular treatment that targets InhA, an enzyme that produces a precursor to mycolic acids[67]. BDQ on the other hand is a last line antibiotic that targets the membrane protein complex of the ATP synthase[68]. The PMF results of ISZ and BDQ show that the *Mycobacterial* membrane behaves as expected regarding the passage of a small molecule through a membrane – showing favorable interactions with the largely hydrophobic BDQ and unfavourable interactions with ISZ (**Figure 3B**). The positive charge present on BDQ could account for the sharp decline in energy at the membrane midplane. The passage of these drugs through a simpler membrane, recapitulating Gram-negative bacteria inner membrane composition (75% PE, 15% PG, 10% CL), is symmetric from the mid-plane of the membrane as expected. With the *Mycobacterial* membrane the interactions of BDQ with the periplasmic leaflet are about 6 kJ/mol larger than for the simple membrane and the *Mycobacterial* cytoplasmic leaflet. There is roughly the same difference between the *Mycobacterial* and simple membranes for ISZ at the mid-membrane region, showing less favorable passage through the membrane. These results suggest that ISZ, a first-line TB drug, is likely to enter the cytoplasm *via* a transporter. This contrasts with the uptake mechanism previously published[69-71], where a mechanism of passive diffusion is reported. In our simulations, when the BDQ starting position was in the bulk solvent, the drug quickly associated with the membrane, as shown in **SI Figure 21**. BDQ shows no strong preference for either leaflet in these simulations.

BDQ has been shown to target the *Mycobacterial* ATP synthase (Rv1304-Rv1311), a membrane protein complex, by inducing large conformational changes which reveal a binding pocket for BDQ. A Cryo-EM structure from *M. smegmatis* (PDB: 7JGC) shows multiple binding sites for BDQ at the interface of the c-subunits and the interface between the a- and c- subunits[31]. There is a highly negatively charged area at this interface (**SI Figure 22A,B**) where the positively charged BDQ[72] interacts. Binding of BDQ to these regions has been found to cause stalling of the rotation of the c-ring, halting ATP synthesis[73]. BDQ has also been shown to localize in host lipid droplets[74].

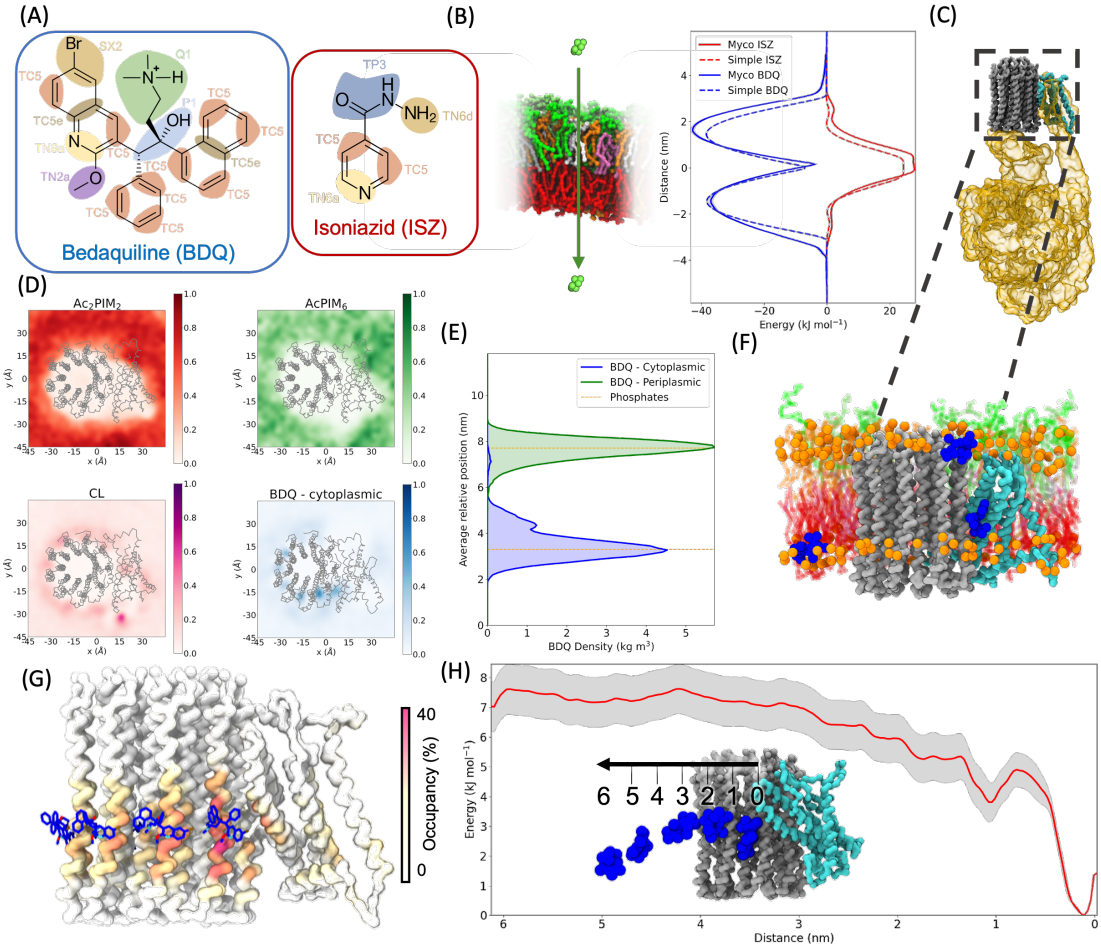

Figure 3: The behavior of the antibiotics with *Mycobacterial* membrane and proteins. (**A**) Chemical structures of BDQ and ISZ with the CG groupings overlaid and bead types shown. (**B**) PMFs of the two antibiotics being pulled through either a *Mycobacterial* or simple membrane in the z-direction. BDQ is shown in blue and ISZ in red, with the *Mycobacterial* membrane results having a solid line and simple membrane having a dashed line. The error is shown in grey. A schematic of the PMF is shown to the left. (**C**) Structure of *Mycobacterium smegmatis* ATP synthase (PDB: 7JG5) with the c-subunits shown in grey, the a-subunit shown in cyan and the other components shown as a gold surface. (**D**) Density in the x and y dimensions of selected lipids and BDQ when starting in the cytoplasmic leaflet relative to the protein shown in grey. (**E**) Density of the phosphates (orange) and BDQ over the course of the

simulations where the antibiotic started in either the periplasmic leaflet (green) or the cytoplasmic leaflet (blue). (**F**) Snapshot of a single simulation containing a *Mtb* ATPase model and 8 x BDQ models showing the main positions BDQ occupied. Phosphates are shown in orange, BDQ shown in blue, c-subunits are shown in grey and the a-subunit is shown in cyan. The lipid sticks are shown in the colors illustrated in **Figure 1A**. (**G**) Comparison of the highest occupancy sites identified with PyLipID (surface) and BDQ from the Cryo-EM structure (PDB: 7JGC) (sticks). (**H**) PMF of BDQ moving through a *Mycobacterial* plasma membrane with the error shown in grey. A schematic of the PMF is shown as an insert.

Throughout 10 simulations of 10 μs, the modeled *Mtb* ATP synthase complex was stable in the asymmetric membrane and there were no significant perturbations of the bilayer by the protein. The lipids of the *Mycobacterial* membrane do not show any strong interactions with the protein (**Figure 3D** and **SI Figure 23**), apart from CL that localizes in the a-subunit and around the c-ring in positions similar to those seen in a previous study[75]. The exact values for CL occupancy of each residue are shown in **SI Figure 25A**. Minimal interactions between BDQ and the ATPase were observed when the drug started in the periplasmic leaflet, but when BDQ started in the cytoplasmic leaflet there was significant occupation of the binding sites as imaged in *M. smegmatis*, **Figures 3D-G** and **SI Figures 22C,D**. There are interactions between the secondary amine group of BDQ and Glu 61 (Glu 65 in *M. smegmatis*) which has been imaged in the determined structure[31], with an occupancy of ~30% of the simulation time on some subunits (**Figure 3G**). The occupancy value averaged over all subunits is shown in **SI Figure 25B**. 3 types of sites reported previously[31] are identified in the simulations. Most interactions are seen through the leading site (46% of the time, K_{off} = 5.2 μs^{-1}) followed by the lagging site (22% of the time, K_{off} = 7.6 μs^{-1}) and finally further interactions around the rotor (36% of the time, K_{off} = 1.2 μs^{-1}, **SI Figure 24**). For the leading site the PMF calculations confirm this as a binding site, giving a moderate energy well of approximately 7 kJ/mol (**Figure 3H**) and making it equivalent to cholesterol binding interaction with a bovine mitochondrial ADP/ATP carrier[76]. Tracking the z-position of the central bead from the antibiotic over the course of the unbiased simulations with the protein shows that the binding sites are occupied to some extent by each of the drug molecules and some are flipped to the outer leaflet from the plasma leaflet, as shown in **SI Figure 22C**.

Resistance mechanisms against BDQ are known to involve the upregulation of MmpL5, a drug efflux pump[77, 78]. This suggests that BDQ must have an entry mechanism into the cytoplasm of the cell and need to access the target – the ATPase

– from the cytoplasm to be effective. This could explain the preference for interaction with the binding site from the cytoplasmic leaflet. When the same simulations were performed starting in either leaflet of the simple Gram-negative membrane (75% PE, 15% PG, 10% CL), there was not a substantial difference in the diffusion coefficients (*Mycobacterial* membrane: 2.2 x 10^{-8} cm^2/s, and simple membrane: 1.7 x 10^{-8} cm^2/s), showing that the antibiotic can move towards its target in either bilayer composition. But, unlike the *Mycobacterial* membrane (**SI Figures 22C,D**), there is no difference between the periplasmic and cytoplasmic leaflets and their interaction with the binding site in the simple symmetric membrane (**SI Figure 26**). This shows the power of modelling an asymmetric membrane to give more nuanced results than symmetric membrane models can provide.

Discussion

Here, we provide models for lipids constituting the *Mycobacterial* plasma membrane focused on the PIM lipids. Understanding how these lipids behave on an individual level and as a constituent of a membrane could provide key insight into the intrinsic resistance of *Mtb* to antibiotics.

In this CG model clustering of ions around these lipids was observed at both the single lipid and bilayer level, probing how this affects the biophysical properties of the bilayer and whether this could be exploited for treatment of TB is an interesting area for future research. The lipids did not cluster together excessively over the timescales studied and all diffused well through the membrane. This confirmed that the *Mycobacterial* cell envelope is dynamic, which could potentially be an important insight into how this cell wall functions. A low membrane bending rigidity compared to a PC and eukaryotic plasma membrane is interesting and could suggest the importance of other cell envelope components in maintaining the shape of the cell.

The simulations confirmed that an asymmetric plasma membrane is stable with a composition of over 50% PIM lipids – a membrane that is unique. As previously mentioned, the integral membrane proteins from *Mtb* are of interest for the development of new antibiotics for TB[8], and this provides a model to simulate proteins in a native lipid environment to determine any key lipid interactions. Here, we have shown that proteins are stable in this bilayer and replicate antibiotic binding that has been seen experimentally[31].

There is room to improve the model, for example incorporating apolar lipids (such as triglycerides[14]), TMM and LM/LAM when the appropriate parameters and relative amounts are available. As the membrane bending rigidity is quite low, incorporation of these other lipids, or indeed changing the concentration of lipids based on future experimental work, will prove interesting. All the AT and CG parameters developed are freely available in CHARMM-GUI Membrane Builder and Martini Maker[79, 80] as well as the scripts utilized in this study for the community to use (see Data Availability section). Future simulations with proteins and probing protein/lipid interactions with atomistic resolution could help further elucidate the role of these complex lipids.

These results are a starting point for building up an entire *Mycobacterial* cell envelope, as has been done for gram-negative bacteria[81]. Other *Mycobacterial* lipids have already been parameterised[82] and in combination could be used to build a model to study the passage of drugs through this barrier to the cell. The *Mycobacterial* cell envelope is known to change at different growth stages during its lifecycle[6, 83-85]. Using CG MD simulations could allow easy modifications of ratios of components – allowing understanding about drug permeability or protein behavior at different stages of infection. This could prove critical to engineering a new treatment regime for TB and non-TB *Mycobacterial* diseases[86].

Data availability: https://github.com/pstansfeld/PIM-lipids
Atomistic systems and CG-membrane set-up can be performed using respectively CHARMM-GUI bilayer builder (https://charmm-gui.org/input/membrane.bilayer) and CHARMM-GUI MARTINI bilayer Maker (https://charmm-gui.org/?doc=input/martini.bilayer)

Acknowledgements

C. M. B. is supported by an MRC studentship (MR/N014294/1). R. A. C. is funded by Wellcome (208361/Z/17/Z). Research in P. J. S.'s lab is funded by Wellcome (208361/Z/17/Z), the MRC (MR/S009213/1) and BBSRC (BB/P01948X/1, BB/R002517/1 and BB/S003339/1). M. C. is supported by the CNRS-MITI grant "Modélisation du vivant" 2020. W. I. is funded by NSF (MCB-2111728). E.F is a Sir Henry Dale Fellow jointly funded by the Wellcome Trust and Royal Society (104193/Z/14/Z and 104193/Z/14/B). M. G. would like to acknowledge the European Union's Horizon 2020 research and innovation program under grant agreement

H2020-PHC-08-2014-643381, TBVAC2020. This work was granted access to the HPC resources of CALMIP supercomputing center (under the allocation 2021-17036) and TGCC Joliot-Curie supercomputer (under the GENCI allocation A0110712941). This project made use of time on ARCHER2 and JADE2 granted via the UK High-End Computing Consortium for Biomolecular Simulation, HECBioSim (http://hecbiosim.ac.uk), supported by EPSRC (grant no. EP/R029407/1). This project also used Athena and Sulis at HPC Midlands+, which were funded by the EPSRC on grants EP/P020232/1 and EP/T022108/1. We thank the University of Warwick Scientific Computing Research Technology Platform for computational access. We thank C. Cooper for fruitful discussions.

Abbreviations

AT:	Atomistic
ATP:	Adenosine triphosphate
BDQ:	Bedaquiline
CL:	Cardiolipin
CG:	Coarse grained
ISZ:	Isoniazid
LAM:	Lipoarabinomannan
LM:	Lipomannan
MD:	Molecular dynamics
Mtb:	*Mycobacterium tuberculosis*
PC:	Phosphatidylcholine
PE:	Phosphatidylethanolamine
PG:	Phosphatidylglycerol
PI:	Phosphatidylinositol
PIMs:	Mannosylated phosphatidylinositol lipids
PIPs:	Phosphatidylinositol phosphates
PME:	Particle mesh Ewald
PMF:	Potential of mean force
TB:	Tuberculosis
TMM:	Trehalose monomycolate

References

1. WHO *Global Tuberculosis Report 2021*; World Health Organization: Geneva, 2021.
2. Horsburgh, C. R.; Barry, C. E.; Lange, C., Treatment of Tuberculosis. *New England Journal of Medicine* **2015,** *373* (22), 2149-2160.
3. WHO The End TB Strategy. https://www.who.int/teams/global-tuberculosis-programme/the-end-tb-strategy (accessed 31-1-22).
4. WHO 1.4 million with tuberculosis, lost out on treatment during first year of COVID-19. https://news.un.org/en/story/2021/03/1087962 (accessed 14/4/22).
5. Chiaradia, L.; Lefebvre, C.; Parra, J.; Marcoux, J.; Burlet-Schiltz, O.; Etienne, G.; Tropis, M.; Daffé, M., Dissecting the mycobacterial cell envelope and defining the composition of the native mycomembrane. *Scientific Reports* **2017,** *7* (1), 12807.
6. Dulberger, C. L.; Rubin, E. J.; Boutte, C. C., The mycobacterial cell envelope — a moving target. *Nature Reviews Microbiology* **2020,** *18* (1), 47-59.
7. Batt, S. M.; Minnikin, D. E.; Besra, G. S., The thick waxy coat of mycobacteria, a protective layer against antibiotics and the host's immune system. *Biochemical Journal* **2020,** *477* (10), 1983-2006.
8. Fullam, E.; Young, R. J., Physicochemical properties and Mycobacterium tuberculosis transporters: keys to efficacious antitubercular drugs? *RSC Medicinal Chemistry* **2021,** *12* (1), 43-56.
9. Sacksteder, K. A.; Protopopova, M.; Barry, C. E., 3rd; Andries, K.; Nacy, C. A., Discovery and development of SQ109: a new antitubercular drug with a novel mechanism of action. *Future Microbiol* **2012,** *7* (7), 823-37.
10. Boudehen, Y.-M.; Faucher, M.; Maréchal, X.; Miras, R.; Rech, J.; Sénèque, O.; Wallat, M.; Demange, P.; Bouet, J.-Y.; Saurel, O.; Catty, P.; Gutierrez, C.; Neyrolles, O., Mycobacterial resistance to zinc poisoning requires assembly of P-ATPase-containing membrane metal efflux platforms. *bioRxiv* **2021**, 2021.10.01.462712.
11. Bansal-Mutalik, R.; Nikaido, H., Mycobacterial outer membrane is a lipid bilayer and the inner membrane is unusually rich in diacyl phosphatidylinositol dimannosides. *Proceedings of the National Academy of Sciences* **2014,** *111* (13), 4958-4963.
12. Gilleron, M.; Quesniaux, V. F. J.; Puzo, G., Acylation State of the Phosphatidylinositol Hexamannosides from *Mycobacterium bovis* Bacillus Calmette Guérin and *Mycobacterium tuberculosis* H37Rv and Its Implication in Toll-like Receptor Response *Journal of Biological Chemistry* **2003,** *278* (32), 29880-29889.
13. Gilleron, M.; Ronet, C.; Mempel, M.; Monsarrat, B.; Gachelin, G.; Puzo, G., Acylation State of the Phosphatidylinositol Mannosides from Mycobacterium bovis Bacillus Calmette Guérin and Ability to Induce Granuloma and Recruit Natural Killer T Cells. *Journal of Biological Chemistry* **2001,** *276* (37), 34896-34904.
14. Jackson, M., The mycobacterial cell envelope-lipids. *Cold Spring Harb Perspect Med* **2014,** *4* (10), a021105.
15. Kalscheuer, R.; Palacios, A.; Anso, I.; Cifuente, J.; Anguita, J.; Jacobs, W. R., Jr; Guerin, M. E.; Prados-Rosales, R., The Mycobacterium tuberculosis capsule: a cell structure with key implications in pathogenesis. *Biochemical Journal* **2019,** *476* (14), 1995-2016.
16. Guerin, M. E.; Korduláková, J.; Alzari, P. M.; Brennan, P. J.; Jackson, M., Molecular Basis of Phosphatidyl-*myo*-inositol Mannoside Biosynthesis and Regulation in Mycobacteria *Journal of Biological Chemistry* **2010,** *285* (44), 33577-33583.

17. Corradi, V.; Sejdiu, B. I.; Mesa-Galloso, H.; Abdizadeh, H.; Noskov, S. Y.; Marrink, S. J.; Tieleman, D. P., Emerging Diversity in Lipid–Protein Interactions. *Chemical Reviews* **2019,** *119* (9), 5775-5848.
18. Xu, P.; Huang, S.; Zhang, H.; Mao, C.; Zhou, X. E.; Cheng, X.; Simon, I. A.; Shen, D.-D.; Yen, H.-Y.; Robinson, C. V.; Harpsøe, K.; Svensson, B.; Guo, J.; Jiang, H.; Gloriam, D. E.; Melcher, K.; Jiang, Y.; Zhang, Y.; Xu, H. E., Structural insights into the lipid and ligand regulation of serotonin receptors. *Nature* **2021,** *592* (7854), 469-473.
19. Jin, R.; He, S.; Black, K. A.; Clarke, O. B.; Wu, D.; Bolla, J. R.; Johnson, P.; Periasamy, A.; Wardak, A.; Czabotar, P.; Colman, P. M.; Robinson, C. V.; Laver, D.; Smith, B. J.; Gulbis, J. M., Ion currents through Kir potassium channels are gated by anionic lipids. *Nature Communications* **2022,** *13* (1), 490.
20. Su, C.-C.; Klenotic, P. A.; Cui, M.; Lyu, M.; Morgan, C. E.; Yu, E. W., Structures of the mycobacterial membrane protein MmpL3 reveal its mechanism of lipid transport. *PLOS Biology* **2021,** *19* (8), e3001370.
21. Herrera, N.; Maksaev, G.; Haswell, E. S.; Rees, D. C., Elucidating a role for the cytoplasmic domain in the Mycobacterium tuberculosis mechanosensitive channel of large conductance. *Scientific Reports* **2018,** *8* (1), 14566.
22. Ingólfsson, H. I.; Melo, M. N.; van Eerden, F. J.; Arnarez, C.; Lopez, C. A.; Wassenaar, T. A.; Periole, X.; de Vries, A. H.; Tieleman, D. P.; Marrink, S. J., Lipid Organization of the Plasma Membrane. *Journal of the American Chemical Society* **2014,** *136* (41), 14554-14559.
23. Pogozheva, I. D.; Armstrong, G. A.; Kong, L.; Hartnagel, T. J.; Carpino, C. A.; Gee, S. E.; Picarello, D. M.; Rubin, A. S.; Lee, J.; Park, S.; Lomize, A. L.; Im, W., Comparative Molecular Dynamics Simulation Studies of Realistic Eukaryotic, Prokaryotic, and Archaeal Membranes. *Journal of Chemical Information and Modeling* **2022,** *62* (4), 1036-1051.
24. Adhyapak, P.; Dong, W.; Dasgupta, S.; Dutta, A.; Duan, M.; Kapoor, S., Lipid Clustering in Mycobacterial Cell Envelope Layers Governs Spatially Resolved Solvation Dynamics. *Chemistry – An Asian Journal* **2022,** *17* (11), e202200146.
25. Newport, T. D.; Sansom, M. S P.; Stansfeld, P. J., The MemProtMD database: a resource for membrane-embedded protein structures and their lipid interactions. *Nucleic Acids Research* **2019,** *47* (D1), D390-D397.
26. Stansfeld, Phillip J.; Goose, Joseph E.; Caffrey, M.; Carpenter, Elisabeth P.; Parker, Joanne L.; Newstead, S.; Sansom, Mark S. P., MemProtMD: Automated Insertion of Membrane Protein Structures into Explicit Lipid Membranes. *Structure* **2015,** *23* (7), 1350-1361.
27. Wassenaar, T. A.; Ingólfsson, H. I.; Böckmann, R. A.; Tieleman, D. P.; Marrink, S. J., Computational Lipidomics with insane: A Versatile Tool for Generating Custom Membranes for Molecular Simulations. *Journal of Chemical Theory and Computation* **2015,** *11* (5), 2144-2155.
28. Wu, E. L.; Cheng, X.; Jo, S.; Rui, H.; Song, K. C.; Dávila-Contreras, E. M.; Qi, Y.; Lee, J.; Monje-Galvan, V.; Venable, R. M.; Klauda, J. B.; Im, W., CHARMM-GUI Membrane Builder toward realistic biological membrane simulations. *Journal of Computational Chemistry* **2014,** *35* (27), 1997-2004.
29. Chavent, M.; Karia, D.; Kalli, A. C.; Domański, J.; Duncan, A. L.; Hedger, G.; Stansfeld, P. J.; Seiradake, E.; Jones, E. Y.; Sansom, M. S. P., Interactions of the EphA2 Kinase Domain with PIPs in Membranes: Implications for Receptor Function. *Structure* **2018,** *26* (7), 1025-1034.e2.

30. Corey, R. A.; Song, W.; Duncan, A. L.; Ansell, T. B.; Sansom, M. S. P.; Stansfeld, P. J., Identification and assessment of cardiolipin interactions with E. coli inner membrane proteins. *Sci Adv* **2021,** *7* (34).
31. Guo, H.; Courbon, G. M.; Bueler, S. A.; Mai, J.; Liu, J.; Rubinstein, J. L., Structure of mycobacterial ATP synthase bound to the tuberculosis drug bedaquiline. *Nature* **2021,** *589* (7840), 143-147.
32. Souza, P. C. T.; Alessandri, R.; Barnoud, J.; Thallmair, S.; Faustino, I.; Grünewald, F.; Patmanidis, I.; Abdizadeh, H.; Bruininks, B. M. H.; Wassenaar, T. A.; Kroon, P. C.; Melcr, J.; Nieto, V.; Corradi, V.; Khan, H. M.; Domański, J.; Javanainen, M.; Martinez-Seara, H.; Reuter, N.; Best, R. B.; Vattulainen, I.; Monticelli, L.; Periole, X.; Tieleman, D. P.; de Vries, A. H.; Marrink, S. J., Martini 3: a general purpose force field for coarse-grained molecular dynamics. *Nature Methods* **2021,** *18* (4), 382-388.
33. Alessandri, R.; Barnoud, J.; Gertsen, A. S.; Patmanidis, I.; de Vries, A. H.; Souza, P. C. T.; Marrink, S. J., Martini 3 Coarse-Grained Force Field: Small Molecules. *Advanced Theory and Simulations* **2022,** *5* (1), 2100391.
34. Borges-Araújo, L.; Souza, P. C. T.; Fernandes, F.; Melo, M. N., Improved Parameterization of Phosphatidylinositide Lipid Headgroups for the Martini 3 Coarse-Grain Force Field. *Journal of Chemical Theory and Computation* **2022,** *18* (1), 357-373.
35. Banerjee, P.; Lipowsky, R.; Santer, M., Coarse-Grained Molecular Model for the Glycosylphosphatidylinositol Anchor with and without Protein. *Journal of Chemical Theory and Computation* **2020,** *16* (6), 3889-3903.
36. Bussi, G.; Donadio, D.; Parrinello, M., Canonical sampling through velocity rescaling. *J Chem Phys* **2007,** *126* (1), 014101.
37. Parrinello, M.; Rahman, A., Polymorphic transitions in single crystals: A new molecular dynamics method. **1981,** *52:12*.
38. Abraham, M. J.; Murtola, T.; Schulz, R.; Páll, S.; Smith, J. C.; Hess, B.; Lindahl, E., GROMACS: High performance molecular simulations through multi-level parallelism from laptops to supercomputers. *SoftwareX* **2015,** *1-2*, 19-25.
39. Barker, J. A.; Watts, R. O., Monte Carlo studies of the dielectric properties of water-like models. *Molecular Physics* **1973,** *26* (3), 789-792.
40. Wu, E. L.; Qi, Y.; Song, K. C.; Klauda, J. B.; Im, W., Preferred Orientations of Phosphoinositides in Bilayers and Their Implications in Protein Recognition Mechanisms. *The Journal of Physical Chemistry B* **2014,** *118* (16), 4315-4325.
41. Lee, J.; Patel, D. S.; Ståhle, J.; Park, S.-J.; Kern, N. R.; Kim, S.; Lee, J.; Cheng, X.; Valvano, M. A.; Holst, O.; Knirel, Y. A.; Qi, Y.; Jo, S.; Klauda, J. B.; Widmalm, G.; Im, W., CHARMM-GUI Membrane Builder for Complex Biological Membrane Simulations with Glycolipids and Lipoglycans. *Journal of Chemical Theory and Computation* **2019,** *15* (1), 775-786.
42. Vanommeslaeghe, K.; Hatcher, E.; Acharya, C.; Kundu, S.; Zhong, S.; Shim, J.; Darian, E.; Guvench, O.; Lopes, P.; Vorobyov, I.; Mackerell, A. D., Jr., CHARMM general force field: A force field for drug-like molecules compatible with the CHARMM all-atom additive biological force fields. *Journal of computational chemistry* **2010,** *31* (4), 671-690.
43. Huang, J.; Rauscher, S.; Nawrocki, G.; Ran, T.; Feig, M.; de Groot, B. L.; Grubmüller, H.; MacKerell, A. D., CHARMM36m: an improved force field for folded and intrinsically disordered proteins. *Nature Methods* **2017,** *14* (1), 71-73.

44. Essmann, U.; Perera, L.; Berkowitz, M. L.; Darden, T.; Lee, H.; Pedersen, L. G., A smooth particle mesh Ewald method. *The Journal of Chemical Physics* **1995,** *103* (19), 8577-8593.
45. Groenewald W, B. M., Croft A, Marrink S-J., Molecular Dynamics of Mycolic Acid Monolayers. *ChemRxiv* **2019**.
46. Fowler, P. W.; Hélie, J.; Duncan, A.; Chavent, M.; Koldsø, H.; Sansom, M. S. P., Membrane stiffness is modified by integral membrane proteins. *Soft Matter* **2016,** *12* (37), 7792-7803.
47. Smith, P.; Lorenz, C. D., LiPyphilic: A Python Toolkit for the Analysis of Lipid Membrane Simulations. *Journal of Chemical Theory and Computation* **2021,** *17* (9), 5907-5919.
48. Bonomi, M.; Bussi, G.; Camilloni, C.; Tribello, G. A.; Banáš, P.; Barducci, A.; Bernetti, M.; Bolhuis, P. G.; Bottaro, S.; Branduardi, D.; Capelli, R.; Carloni, P.; Ceriotti, M.; Cesari, A.; Chen, H.; Chen, W.; Colizzi, F.; De, S.; De La Pierre, M.; Donadio, D.; Drobot, V.; Ensing, B.; Ferguson, A. L.; Filizola, M.; Fraser, J. S.; Fu, H.; Gasparotto, P.; Gervasio, F. L.; Giberti, F.; Gil-Ley, A.; Giorgino, T.; Heller, G. T.; Hocky, G. M.; Iannuzzi, M.; Invernizzi, M.; Jelfs, K. E.; Jussupow, A.; Kirilin, E.; Laio, A.; Limongelli, V.; Lindorff-Larsen, K.; Löhr, T.; Marinelli, F.; Martin-Samos, L.; Masetti, M.; Meyer, R.; Michaelides, A.; Molteni, C.; Morishita, T.; Nava, M.; Paissoni, C.; Papaleo, E.; Parrinello, M.; Pfaendtner, J.; Piaggi, P.; Piccini, G.; Pietropaolo, A.; Pietrucci, F.; Pipolo, S.; Provasi, D.; Quigley, D.; Raiteri, P.; Raniolo, S.; Rydzewski, J.; Salvalaglio, M.; Sosso, G. C.; Spiwok, V.; Šponer, J.; Swenson, D. W. H.; Tiwary, P.; Valsson, O.; Vendruscolo, M.; Voth, G. A.; White, A.; The, P. c., Promoting transparency and reproducibility in enhanced molecular simulations. *Nature Methods* **2019,** *16* (8), 670-673.
49. Buchoux, S., FATSLiM: a fast and robust software to analyze MD simulations of membranes. *Bioinformatics* **2017,** *33* (1), 133-134.
50. Hunter, J. D., Matplotlib: A 2D Graphics Environment. *Computing in Science & Engineering* **2007,** *9* (3), 90-95.
51. Graham, J. A.; Essex, J. W.; Khalid, S., PyCGTOOL: Automated Generation of Coarse-Grained Molecular Dynamics Models from Atomistic Trajectories. *Journal of Chemical Information and Modeling* **2017,** *57* (4), 650-656.
52. Kim, S.; Lee, J.; Jo, S.; Brooks III, C. L.; Lee, H. S.; Im, W., CHARMM-GUI ligand reader and modeler for CHARMM force field generation of small molecules. *Journal of Computational Chemistry* **2017,** *38* (21), 1879-1886.
53. Waterhouse, A.; Bertoni, M.; Bienert, S.; Studer, G.; Tauriello, G.; Gumienny, R.; Heer, F. T.; de Beer, T. A P.; Rempfer, C.; Bordoli, L.; Lepore, R.; Schwede, T., SWISS-MODEL: homology modelling of protein structures and complexes. *Nucleic Acids Research* **2018,** *46* (W1), W296-W303.
54. Sievers, F.; Wilm, A.; Dineen, D.; Gibson, T. J.; Karplus, K.; Li, W.; Lopez, R.; McWilliam, H.; Remmert, M.; Söding, J.; Thompson, J. D.; Higgins, D. G., Fast, scalable generation of high-quality protein multiple sequence alignments using Clustal Omega. *Molecular Systems Biology* **2011,** *7* (1), 539.
55. Kroon, P. C. Aggregate, automate, assemble. University of Groningen, 2020.
56. Nugent, T.; Jones, D. T., Membrane protein orientation and refinement using a knowledge-based statistical potential. *BMC Bioinformatics* **2013,** *14* (1), 276.
57. Song, W.; Corey, R. A.; Ansell, T. B.; Cassidy, C. K.; Horrell, M. R.; Duncan, A. L.; Stansfeld, P. J.; Sansom, M. S. P., PyLipID: A Python Package for Analysis of Protein–Lipid

783 Interactions from Molecular Dynamics Simulations. *Journal of Chemical Theory and*
784 *Computation* **2022,** *18* (2), 1188-1201.
785 58. Corey, R. A.; Vickery, O. N.; Sansom, M. S. P.; Stansfeld, P. J., Insights into Membrane
786 Protein–Lipid Interactions from Free Energy Calculations. *Journal of Chemical Theory and*
787 *Computation* **2019,** *15* (10), 5727-5736.
788 59. Souaille, M.; Roux, B. t., Extension to the weighted histogram analysis method:
789 combining umbrella sampling with free energy calculations. *Computer Physics*
790 *Communications* **2001,** *135* (1), 40-57.
791 60. Hub, J. S.; de Groot, B. L.; van der Spoel, D., g_wham—A Free Weighted Histogram
792 Analysis Implementation Including Robust Error and Autocorrelation Estimates. *Journal of*
793 *Chemical Theory and Computation* **2010,** *6* (12), 3713-3720.
794 61. Schmalhorst, P. S.; Deluweit, F.; Scherrers, R.; Heisenberg, C.-P.; Sikora, M.,
795 Overcoming the Limitations of the MARTINI Force Field in Simulations of Polysaccharides.
796 *Journal of Chemical Theory and Computation* **2017,** *13* (10), 5039-5053.
797 62. Hoffmann, C.; Leis, A.; Niederweis, M.; Plitzko, J. M.; Engelhardt, H., Disclosure of
798 the mycobacterial outer membrane: Cryo-electron tomography and vitreous sections reveal
799 the lipid bilayer structure. *Proceedings of the National Academy of Sciences* **2008,** *105* (10),
800 3963-3967.
801 63. Zuber, B.; Chami, M.; Houssin, C.; Dubochet, J.; Griffiths, G.; Daffé, M., Direct
802 visualization of the outer membrane of mycobacteria and corynebacteria in their native state.
803 *J Bacteriol* **2008,** *190* (16), 5672-5680.
804 64. Adhyapak, P.; Srivatsav, A. T.; Mishra, M.; Singh, A.; Narayan, R.; Kapoor, S.,
805 Dynamical Organization of Compositionally Distinct Inner and Outer Membrane Lipids of
806 Mycobacteria. *Biophysical Journal* **2020,** *118* (6), 1279-1291.
807 65. Hughes, A. V.; Patel, D. S.; Widmalm, G.; Klauda, J. B.; Clifton, L. A.; Im, W., Physical
808 Properties of Bacterial Outer Membrane Models: Neutron Reflectometry & Molecular
809 Simulation. *Biophysical Journal* **2019,** *116* (6), 1095-1104.
810 66. Friedman, R., Membrane-Ion Interactions. *The Journal of membrane biology* **2018,** *251*
811 (3), 453-460.
812 67. Anderson, R. J.; Groundwater, P. W.; Todd, A.; Worsley, A. J., *Antibacterial agents :*
813 *chemistry, mode of action, mechanisms of resistance and clinical applications*. Wiley-
814 Blackwell: Chichester, 2012; p 378.
815 68. Dartois, V. A.; Rubin, E. J., Anti-tuberculosis treatment strategies and drug
816 development: challenges and priorities. *Nature Reviews Microbiology* **2022**.
817 69. Bardou, F.; Raynaud, C.; Ramos, C.; Lanéelle, M. A.; Lanéelle, G., Mechanism of
818 isoniazid uptake in Mycobacterium tuberculosis. *Microbiology* **1998,** *144* (9), 2539-2544.
819 70. Unissa, A. N.; Subbian, S.; Hanna, L. E.; Selvakumar, N., Overview on mechanisms of
820 isoniazid action and resistance in Mycobacterium tuberculosis. *Infection, Genetics and*
821 *Evolution* **2016,** *45*, 474-492.
822 71. Jackson, M.; Raynaud, C.; Lanéelle, M.-A.; Guilhot, C.; Laurent-Winter, C.;
823 Ensergueix, D.; Gicquel, B.; Daffé, M., Inactivation of the antigen 85C gene profoundly affects
824 the mycolate content and alters the permeability of the Mycobacterium tuberculosis cell
825 envelope. *Molecular Microbiology* **1999,** *31* (5), 1573-1587.
826 72. Haagsma, A. C.; Podasca, I.; Koul, A.; Andries, K.; Guillemont, J.; Lill, H.; Bald, D.,
827 Probing the interaction of the diarylquinoline TMC207 with its target mycobacterial ATP
828 synthase. *PLoS One* **2011,** *6* (8), e23575-e23575.

829 73. Sarathy, J. P.; Gruber, G.; Dick, T., Re-Understanding the Mechanisms of Action of the
830 Anti-Mycobacterial Drug Bedaquiline. *Antibiotics (Basel)* **2019,** *8* (4), 261.
831 74. Greenwood Daniel, J.; Dos Santos Mariana, S.; Huang, S.; Russell Matthew, R. G.;
832 Collinson Lucy, M.; MacRae James, I.; West, A.; Jiang, H.; Gutierrez Maximiliano, G.,
833 Subcellular antibiotic visualization reveals a dynamic drug reservoir in infected macrophages.
834 *Science* **2019,** *364* (6447), 1279-1282.
835 75. Duncan, A. L.; Robinson, A. J.; Walker, J. E., Cardiolipin binds selectively but transiently
836 to conserved lysine residues in the rotor of metazoan ATP synthases. *Proceedings of the*
837 *National Academy of Sciences* **2016,** *113* (31), 8687-8692.
838 76. Corey, R. A.; Stansfeld, P. J.; Sansom, M. S. P., The energetics of protein-lipid
839 interactions as viewed by molecular simulations. *Biochem Soc Trans* **2020,** *48* (1), 25-37.
840 77. Briffotaux, J.; Huang, W.; Wang, X.; Gicquel, B., MmpS5/MmpL5 as an efflux pump in
841 Mycobacterium species. *Tuberculosis* **2017,** *107*, 13-19.
842 78. Degiacomi, G.; Sammartino, J. C.; Sinigiani, V.; Marra, P.; Urbani, A.; Pasca, M. R., In
843 vitro Study of Bedaquiline Resistance in Mycobacterium tuberculosis Multi-Drug Resistant
844 Clinical Isolates. *Frontiers in Microbiology* **2020,** *11*.
845 79. Qi, Y.; Ingólfsson, H. I.; Cheng, X.; Lee, J.; Marrink, S. J.; Im, W., CHARMM-GUI Martini
846 Maker for Coarse-Grained Simulations with the Martini Force Field. *Journal of Chemical*
847 *Theory and Computation* **2015,** *11* (9), 4486-4494.
848 80. CHARMM-GUI, Martini Maker now supports Martini 3. @CharmmGui, Ed. Twitter:
849 2022.
850 81. Im, W.; Khalid, S., Molecular Simulations of Gram-Negative Bacterial Membranes
851 Come of Age. *Annual Review of Physical Chemistry* **2020,** *71* (1), 171-188.
852 82. Augenstreich, J.; Haanappel, E.; Ferré, G.; Czaplicki, G.; Jolibois, F.; Destainville, N.;
853 Guilhot, C.; Milon, A.; Astarie-Dequeker, C.; Chavent, M., The conical shape of DIM lipids
854 promotes *Mycobacterium tuberculosis* infection of macrophages. *Proceedings of the National*
855 *Academy of Sciences* **2019,** *116* (51), 25649-25658.
856 83. Queiroz, A.; Riley, L. W., Bacterial immunostat: Mycobacterium tuberculosis lipids and
857 their role in the host immune response. *Rev Soc Bras Med Trop* **2017,** *50* (1), 9-18.
858 84. Abrahams, K. A.; Besra, G. S., Synthesis and recycling of the mycobacterial cell
859 envelope. *Current Opinion in Microbiology* **2021,** *60*, 58-65.
860 85. Modak, B.; Girkar, S.; Narayan, R.; Kapoor, S., Mycobacterial Membranes as
861 Actionable Targets for Lipid-Centric Therapy in Tuberculosis. *Journal of Medicinal Chemistry*
862 **2022,** *65* (4), 3046-3065.
863 86. Dartois, V.; Dick, T., Drug development challenges in nontuberculous mycobacterial
864 lung disease: TB to the rescue. *Journal of Experimental Medicine* **2022,** *219* (6).
865